NIST-GCR-97-729

PREDICTION OF FIRE DYNAMICS

John de Ris

Factory Mutual Research Corporation
Norwood, MA 02062

United States Department of Commerce
Technology Administration
National Institute of Standards and Technology

NIST-GCR-97-729

PREDICTION OF FIRE DYNAMICS

Prepared for
U.S. Department of Commerce
Building and Fire Research Laboratory
National Institute of Standards and Technology
Gaithersburg, MD 20899

By
John de Ris
Factory Mutual Research Corporation
Norwood, MA 02062

June 1995
Issued October 1997

Notice

This report was prepared for the Building and Fire Research Laboratory of the National Institute of Standards and Technology under grant number 60NANB1D1177. The statement and conclusions contained in this report are those of the authors and do not necessarily reflect the views of the National Institute of Standards and Technology or the Building and Fire Research Laboratory.

PREDICTION OF FIRE DYNAMICS

FINAL REPORT

AND

THIRD CALENDAR QUARTERLY REPORT

July 1, 1994 - August 28, 1994

NIST Grant No: 60NANB1D1177

June 1995

John de Ris

Principal Investigator

Factory Mutual Research Corporation

Norwood, MA 02062

INTRODUCTION

This report summarizes accomplishments of a Factory Mutual Research Corporation (FMRC) project on the Prediction of Fire Dynamics for the NIST grant period indicated. Work performed under a subcontract by Professor H.W. Emmons on Transient Ceiling Jet Heat Transfer is described as part of Task 1, Prediction of Fires in Buildings. This task has developed new practical expressions for heat transfer rates between the fire-induced ceiling-jet and the ceiling surface, so that the rate of increase in ceiling temperature can be predicted more reliably.

The accomplishments of three tasks performed at FMRC are then presented in summaries of Tasks 2, 4, and 5. In Tasks 2 and 4, considerable progress has been made in the formulation of similarity relationships for gas temperature and soot layer thickness profiles in real-scale wall fires. We believe that these similarity relationships can be exploited to describe turbulent buoyant flames on vertical surfaces more accurately than ever.

All of this work is aimed at the development of submodels or algorithms that can be used in NIST/BFRL comprehensive computer fire models. The FMRC tasks have previously led to the development of practical smoke-point measurement techniques for solid combustible materials, as described in a paper presented at the 4th International Symposium on Fire Safety Science, Ottawa, June 1994.

TASK 1: Prediction of Fire in Buildings (H.W. Emmons, Gordon McKay Professor of Mechanical Engineering Emeritus, Abbott and James Lawrence Professor Engineering Emeritus)

Transient Ceiling Jet Heat Transfer

A ceiling jet heat transfer theory should be analyzed along with the dynamics.[1,2] At present such complete analyses do not agree as well with experiment as when the dynamics are assumed constant.[3] In the following the dynamics are assumed to be known and are set at the mean values of velocity u, depth δ, and mass flow per unit width $\dot{m}$.

Under these conditions, the ceiling jet energy equations reduce to temperature equations describing the heat conduction and radiation from the ceiling jet to the ceiling and to ambient temperature objects below while the ceiling radiates to the ambient.

The equations are: for the ceiling jet,

$$\rho_s\delta_s c_p \frac{\partial T_s}{\partial t} + u\rho_s\delta_s c_{ps}\frac{\partial T_s}{\partial x} + h(T_s - T_w) + h_a(T_s - T_a) = 0 \qquad 1$$

for the ceiling,

$$\rho_w\delta_w c_p \frac{\partial T_w}{\partial t} \qquad - h(T_s - T_w) + h_{wa}(T_w - T_a) = 0 \qquad 2$$

Although the open end of a corridor has no direct thermal effect on upstream heat transfer, it is a useful length scale for nondimensionalization. Thus introduce the variables

$$x,\ ut,\ \theta_s = \frac{T_s - T_a}{T_0 - T_a},\quad \theta_w = \frac{T_w - T_a}{T_0 - T_a} \qquad \text{variables} \qquad 3$$

$$p_s = \frac{h}{c_p\dot{m}},\quad p_a = \frac{h_a}{c_p\dot{m}},\quad p_w = \frac{h}{c_{pw}\rho_w\delta_w u},\quad p_{wa} = \frac{h_{wa}}{c_{pw}\rho_w\delta_w u} \qquad \text{parameters} \qquad 4$$

to get

$$\frac{\partial\theta_s}{\partial ut} + \frac{\partial\vartheta_s}{\partial x} + p_s(\theta_s - \theta_w) + p_a\theta_s = 0 \qquad [m^{-1}] \qquad 5$$

$$\frac{\partial\theta_w}{\partial ut} \qquad - p_w(\theta_s - \theta_w) + p_{wa}\theta_w = 0 \qquad [m^{-1}] \qquad 6$$

with boundary conditions

$$\theta_s(x,0) = 0 \qquad \theta_s(0,ut) = 1 \qquad 7$$

$$\theta_w(x,0) = 0 \qquad 8$$

where the length L has been canceled out of equations 5 and 6.

The solution obtained using LaPlace transforms is:

$$\theta_s = e^{-(p_s+p_w)x_s}\{e^{-(p_w+p_{wa})(ut-x)} I_0(2\sqrt{p_s p_w x(ut-x)}) + (p_w + p_{wa})\int_0^{ut-x} e^{-(p_w+p_{wa})z} I_0(2\sqrt{p_s p_w xz})dz\ \}\ U(ut-x) \qquad 9$$

$$\theta_w = e^{-(p_s+p_w)x}\ p_w\int_0^{ut-x} e^{-(p_w+p_{wa})z} I_0(2\sqrt{p_s p_w xz})dz\ U(ut-x) \qquad 10$$

$$\theta_s - \theta_w = e^{-(p_s+p_a)x}\{e^{-(p_w+p_{wa})(ut-x)} I_0(2\sqrt{p_s p_w x(ut-x)}) + p_{wa}\int_0^{ut-x} e^{-(p_w+p_{wa})z} I_0(2\sqrt{p_s p_w xz})dz\ \}\ U(ut-x) \qquad 11$$

The corresponding local and average heat transfer rates are
ceiling jet to ceiling

$$\dot{q}'' = h(T_0 - T_a)(\theta_a - \theta_w) \quad 12$$

$$Q = h(T_0 - T_a)L'\overline{(\theta_a - \theta_w)} \quad 13$$

ceiling jet to ambient below

$$\dot{q}'' = h_a(T_0 - T_a)\theta_a \quad 14$$

$$Q = h_a(T_0 - T_a)L'\overline{\theta_s} \quad 15$$

ceiling to ambient below

$$\dot{q}'' = h_{wa}(T_0 - T_a)\theta_w \quad 16$$

$$Q = h_{wa}(T_0 - T_{wa})L'\overline{\theta_w} \quad 17$$

where the overbar indicates the arithmetic average over the effective length L`

$$L' = \begin{cases} L \text{ if } ut > L \\ x \text{ if } x < L \text{ and } ut > x \end{cases} \quad 18$$

Analysis of Results

Case I An important case has a ceiling held at ambient temperature $\theta_w = 0$. The general solution reduces to

$$\theta_a = e^{-(p_s + p_a)x}\ U(ut-x) \quad 19$$

and the heat transfer rates ceiling jet to ceiling and ambient are:

$$\dot{q}'' = (h + h_a)(T_0 - T_a)\theta_a \quad 20$$

$$Q = (h + h_a)(T_0 - T_a)L'\theta_a = (h + h_a)L'\overline{\Delta T} \quad 21$$

where

$$\overline{\Delta T} = \frac{(T_s(0) - T_a) - (T_s(L) - T_a)}{\ln \frac{T_s(0) - T_a}{T_s(L) - T_a}} \quad 22$$

Case II

It is instructive to examine a specific case of ceiling jet heat transfer in a corridor. The case chosen is as follows: Fire gases at 800 K issues at .5 kg/sec into a corridor 3m wide ($\dot{m}$ = .1667kg/sec m) and length L = 100m. The ceiling is initially at 300 K but heats up with time. The ambient temperature below is at T_a = 300 K and remains so. The properties of the ceiling were taken as 1/2 " thick gypsum board for which $\rho_w \delta_w c_{pw} = 1024$ J/m^{2}K

The mean ceiling jet properties were taken at T_{ave}= 550 K with a density of $\rho_a = \rho_{550} = .642$kg/m^3 which implies an effective gravity of g' = g$\Delta\rho/\rho$ = 4.459m/sec^2. Following Zukoski [4], the ceiling jet volume flow per unit width $Q = \dot{m}/\rho_a$ = .260m^2/sec which implies a jet velocity of $u = (g'Q)^{1/3}$ = 1.050m/sec and a jet depth of $\delta_a = (Q^2/g')^{1/3}$ = .247m. Finally the connective heat transfer to the ceiling is given by Nu = .013 Re, Zukoski[5]. The thermal conductivity and viscosity of the ceiling jet was taken as that of air (mostly N_2) at the mean film temperature of 425 K. Adding a linearized radiative heat transfer coefficient results in:

h = 28.8w/m^{2}K which implies p_a = .171 m^{-1} and p_w =.00293 m^{-1}.
the remaining radiative heat transfer coefficients are

h_a = 12.9 giving p_a = .0763 m^{-1}
h_{wa}=7.00 giving p_{wa}=.00055 m^{-1}

The solution for the ceiling jet temperature, θ_a, equation 9 is presented as figure 1, and for the ceiling, θ_w, equation 10 as figure 2. The ceiling jet to ceiling temperature difference, $\theta_a - \theta_w$, equation 11 figure 3, shows the local heat transfer rate from the ceiling jet to the ceiling, equation 12. As expected the

heat transfer rate is large at the beginning of the corridor and at early times and falls off approximately exponentially with time and location,

For some purposes only the mean heat transfer rates are needed, equation 13, which is shown as the average temperature difference for length x and time ut in figure 4 for the specific case of a 10 meter long corridor. For this specific case it shows that the ceiling jet advances to the end of this corridor in time t = 9.5sec after which the mean temperature difference in the corridor falls as the ceiling heats up

Figure 5 shows that the mean heat transfer rate falls rapidly while the ceiling jet first advances but falls slowly for a long time thereafter. .

Since by plotting all of the temperature variations vs x on semilog paper show only slightly bent lines, it would be expected that the frequently used log mean of the end temperature differences would give a rather good simple approximation to the over all heat transfer. As the points x in figure 5 shows, the log mean approach gives heat transfers that are too high up to 42%. If experimental data identical to the present theory were measured and were interpreted using the log mean temperature difference, the maximum would be only about 20%.

Drop from ceiling.

The ceiling jet as it flows down a long corridor has its buoyancy becomes so small that it cannot remain at the ceiling against miscellaneous drafts, etc. The theory of this process is very complex and has not been adequately explored. To see the general effect, it was assumed that the ceiling jet could not remain at the ceiling beyond $\theta_u = .01$, i.e. for the present case the ceiling jet temperature is within 5 K of the ambient. From figure 1 it is seen that the $\theta_u = .01$ point moves forward much more slowly than the normal jet velocity. This is shown in figure 6.

Other heat transfer coefficients.

The local heat transfer rate between the ceiling jet and the ceiling depends on the actual local temperature difference between them. .Since the actual ceiling jet temperature is given by a formula at least as complex as in this paper, it has been suggested that the ceiling jet heat transfer coefficient be based upon an adiabatic ceiling jet temperature defined as the ceiling jet with no heat transfer to the ceiling. This "adiabatic" temperature is a simple exponential Cooper[5] For the present case, the ceiling jet actual temperature and the arbitrarily selected adiabatic temperature are compared in figure 6. The resultant heat transfer coefficients would be very different. For example, if the ceiling had a temperature distribution equal to the adiabatic ceiling jet while the actual temperature of the ceiling jet were the lower line in figure 6, the adiabatic approach would be no heat transfer while in fact it is quite large. The use of the simpler adiabatic temperature can of course reproduce exactly the data from which it was obtained and is useful in fire calculations which are close to the conditions of the original test.

1 Alpert R, Turbulent Ceiling Jet Induced by Large Scale Fires. Comb. Sci.Tech 11 p197 1975
2 Emmons H.W. The Ceiling Jet in Fires NIST-GCR-90-102-1990
3 Chobotov M.V. Gravity Currents with Heat Transfer Effects PhD theses CIT 1987
4 Zukoski E. Personal Communication (Fr = 1)
5 Zukoski E. Heat Tramsfer in Unwanted Fires ASME-JSME Thermal Eng. Conf. Honolulu 1987
6. Cooper L. Woodlouse A The Buoyant Plume Driven Adiabatic Ceiling Temperature Revisited. ASME Jour.Heat Trans. 108 p822 1986
7 Abramowitz M. Stegun I Hdbk Math. Func. NBS App Math. Series 55 1965.

c_p specific heat
g standard gravity
g' modified gravity
h heat transfer coefficient
I_0 modified Bessel function[7]
L corridor length
L' length x or L
$\dot{m}$ mass flow/width
p parameter
$\dot{q}$" local heat flux
Q heat transfer in L'/width
t time
T temperature
u velocity
U(z) = 1 if z>0, = 0 if z<0
x distance along corridor
z integration variable

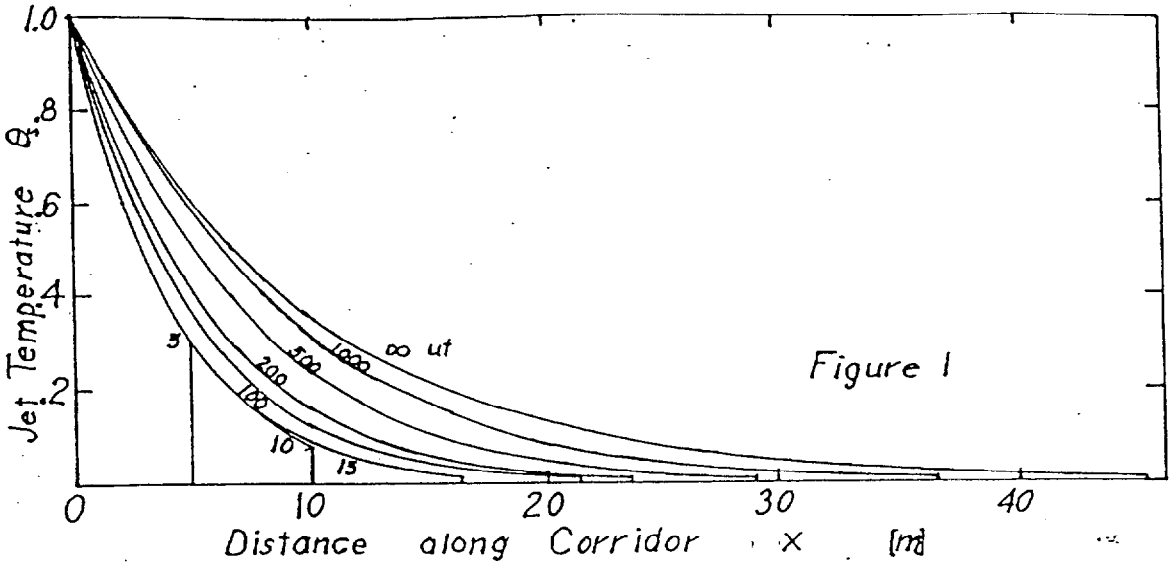

Figure 1

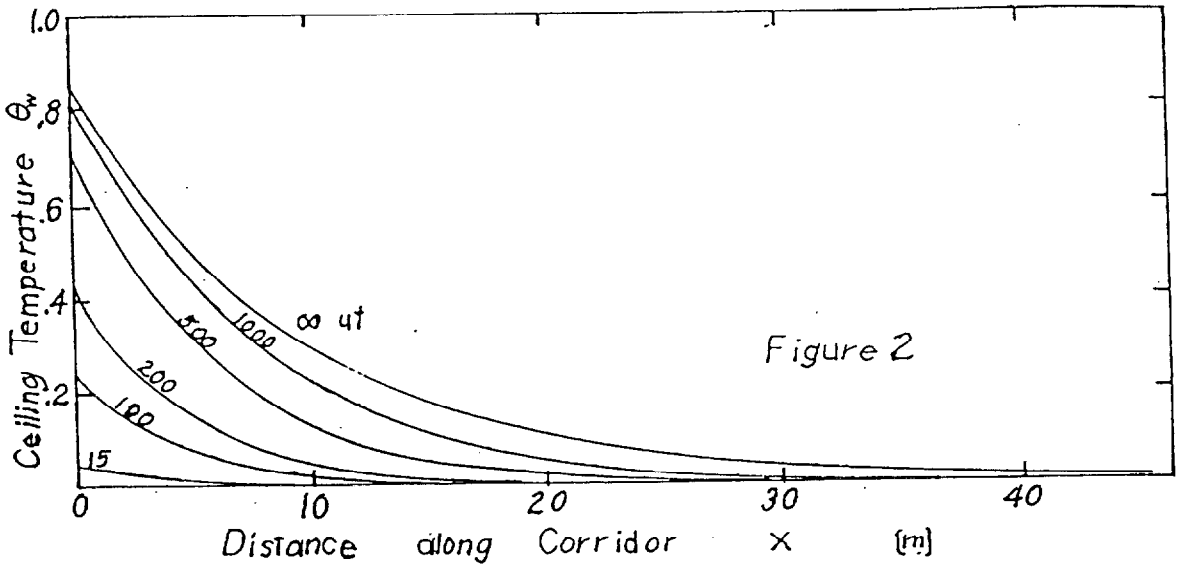

Figure 2

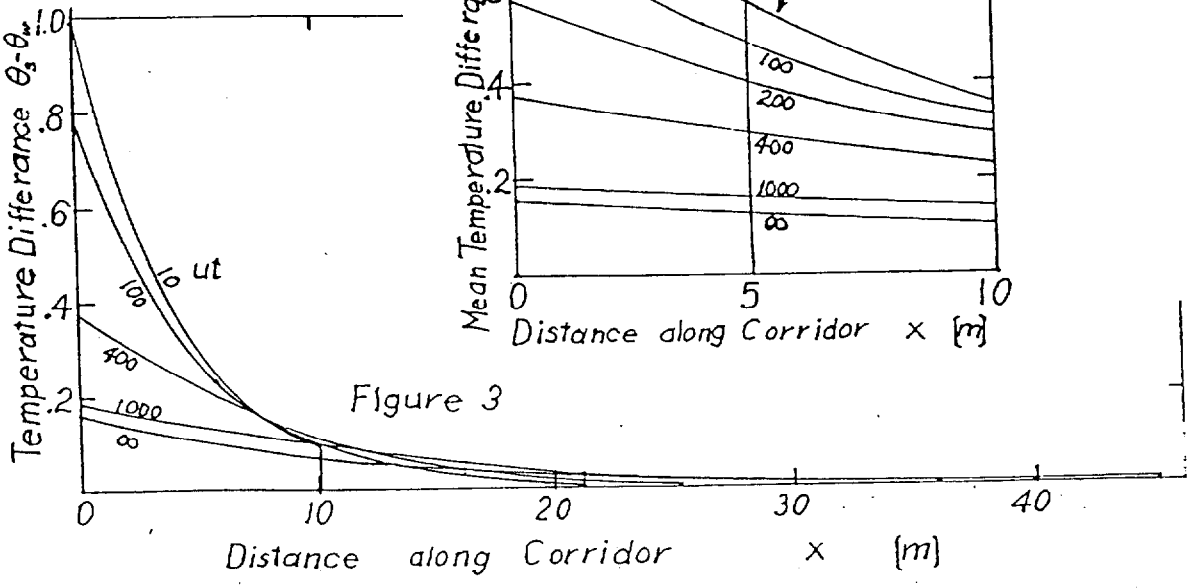

Figure 3

Figure 4

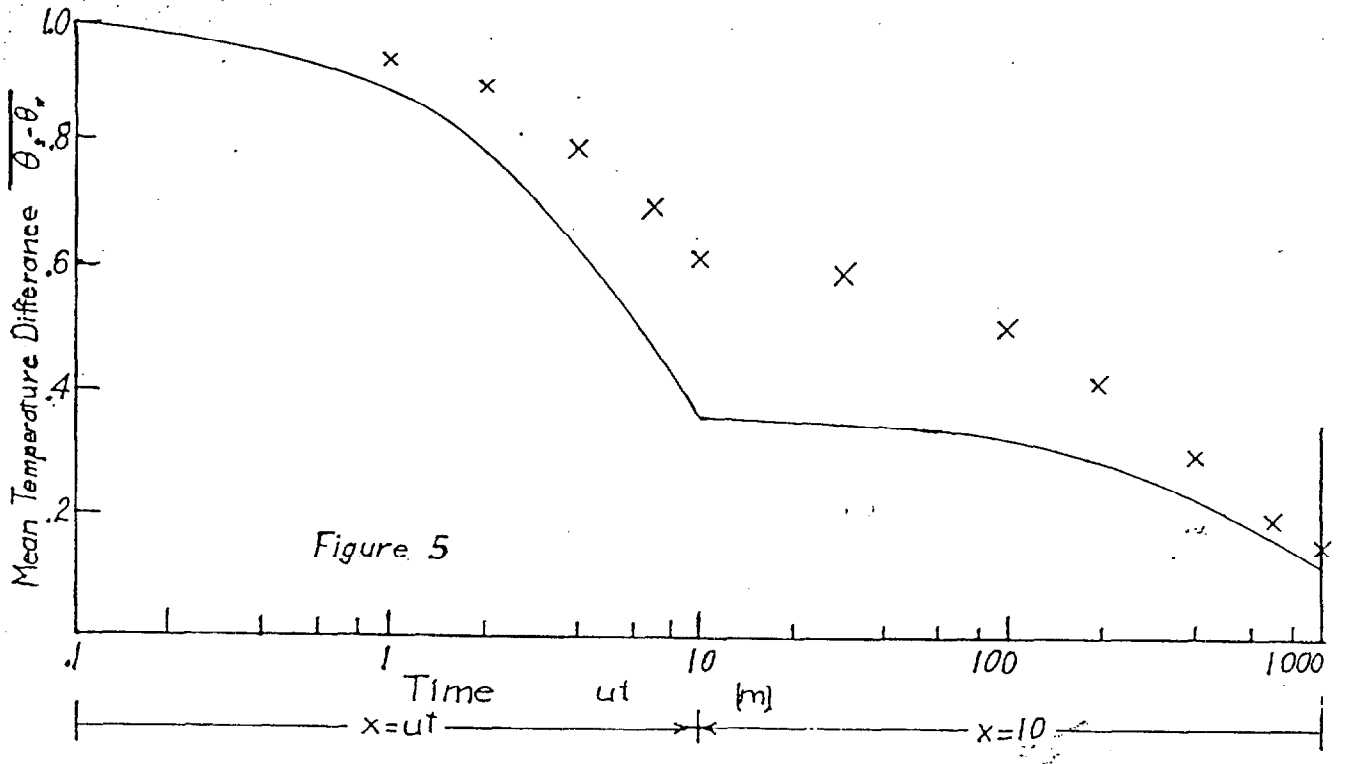

Figure 5

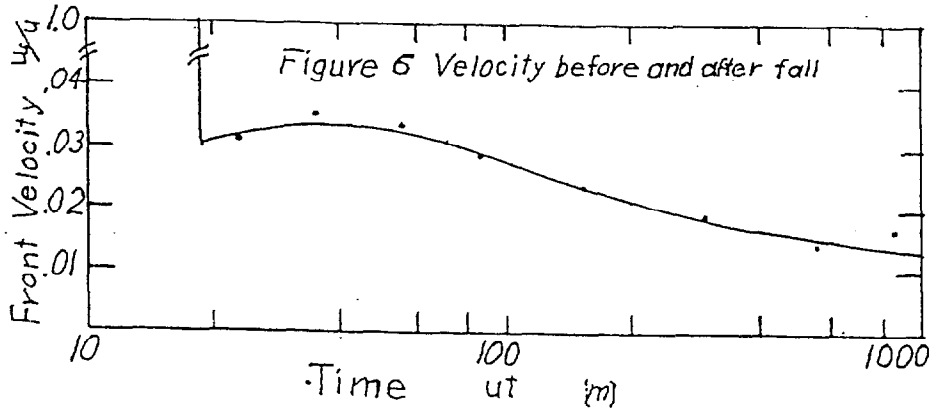

Figure 6 Velocity before and after fall

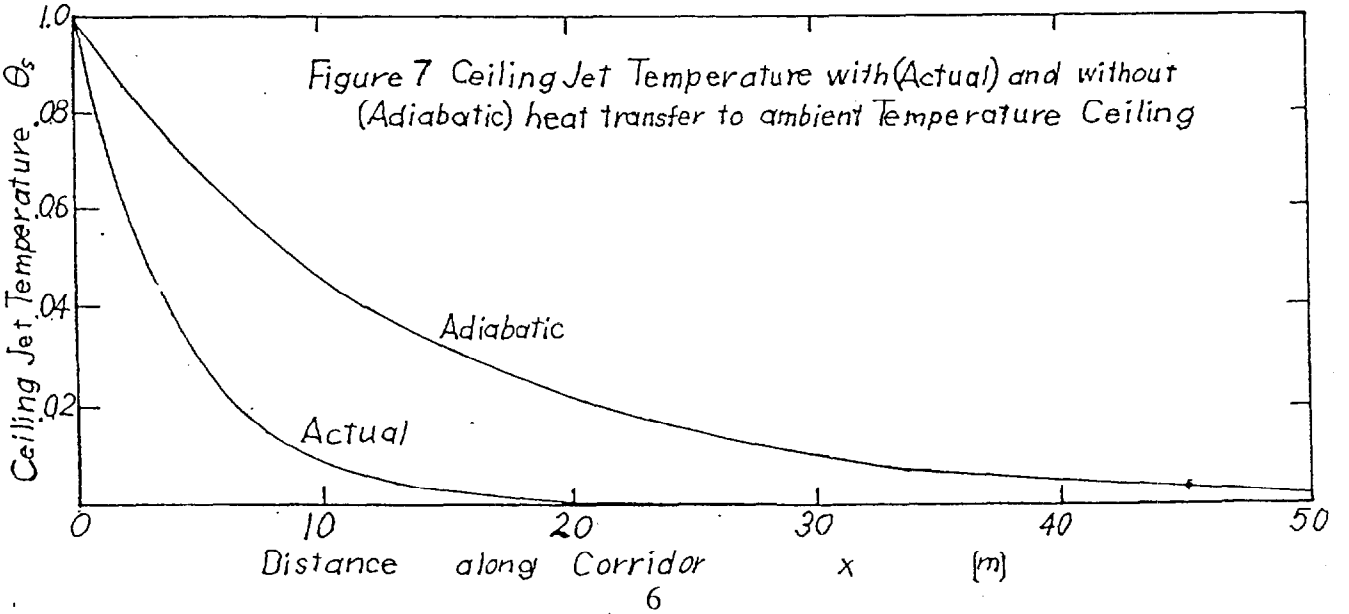

Figure 7 Ceiling Jet Temperature with (Actual) and without (Adiabatic) heat transfer to ambient Temperature Ceiling

TASK 2: Models for Turbulent Flame Chemistry and Radiation (J. de Ris)
and
TASK 4: Soot and CO Oxidation in Buoyant Turbulent Diffusion Flames (L. Orloff)

The objective of Task 2 is to develop models for predicting 1) wall fire radiative feedback to the fuel surface, which controls wall fire burning rates, and 2) the combined soot and CO oxidation which controls the release of incomplete (toxic) products of combustion (soot, CO, etc.) and radiation from buoyant turbulent diffusion flames. Task 4 has the objective of providing experimental data for the development of these models.

Considerable progress has been achieved during the past year towards the formulation of similarity relationships that may be very encouraging to fire modelers. Analysis of temperature and soot layer thickness profiles together with Markstein's[1,2] radiant extinction measurements show that the profiles remain geometrically similar for a fixed overall fuel to entrained air equivalence ratio corresponding to a fuel mass transfer rate, $\dot{m}''$, which increases with the square root of height, Z. For additional detailed descriptions of the measurement and data-reduction techniques that were employed to reach this conclusion, see Appendix A-E.

Various pyrolysis zone heights were simulated by supplying propylene to up to ten 132 mm high and 320 mm wide water-cooled sintered-metal gas burners. The forward heat transfer zone was simulated by a 660 mm high water-cooled heat transfer plate mounted above the gas burners. The flow was maintained two-dimensional by 150 mm deep water-cooled side walls attached to the burner apparatus over its entire height.

The thickness of the soot layer, δ_s, was measured by inserting arrays of 5 mm glass rods into the flames perpendicular to the wall surface and rapidly withdrawing them after a two second exposure to the flames. The soot layer thickness was determined from the average length of soot deposit on ten rods.

Figure 1 shows the length ratio, Z/δ_s, correlated against the inverse modified equivalence ratio $\rho_A(2gZ)^{1/2}/(\dot{m}''-\dot{m}''_o)$. The modification of the equivalence ratio is required because the soot vanishes and the flames become blue for mass transfer rates less than $\dot{m}''_o$=4 g/m^{2}s. As a result of wall cooling and dilution by the products of combustion at low mass transfer rates, the data show that the cut-off, $\dot{m}''_o$, is independent of Z. The turbulent motion typically transports the luminous soot (e.g. visible flames) out into the incoming air all the way to where the mean gas temperature drops to around 1000K. The correlation says that the soot layer thickness is

proportional to Z for a given ratio of entrained air, $\rho_A(2gZ^3)^{1/2}$ to supplied fuel $\dot{m}''Z$ above its blue flame value $\dot{m}''_oZ$. The correlation extends over a very wide range of flame equivalence ratios.

Temperature profiles across the flame boundary layer were measured by a thermocouple rake consisting of 15 insulated Chromel-Alumel thermocouples inside 1.6 mm diameter Inconel sheaths spaced 12.6 mm on center and protruding 1 cm downward into the rising flow. The measured temperatures inside the flame were significantly depressed by radiation heat loss. On the other hand, the thermocouple temperatures outside the flame were significantly increased by radiant heat transfer from the flame. We corrected for both these effects with a simple heat transfer model to obtain the correlations shown in Figure 2. The vertical dashed line at $y/\delta=1$ shows the boundary of the soot layer occurring at temperatures near T=1000K. Inside the soot layer, the presence of cold fuel is seen by the temperature drop near the wall. Outside the soot layer, the mixing of combustion products with the entrained air causes the corrected temperatures to asymptotically approach the ambient temperature as y/δ increases. These outer temperature profiles correlate reasonably well when plotted against $(y-\delta)/Z$.

Markstein[2] reports measurements of the extinction of infrared radiation, ε_o, by soot (at wavelengths λ_o = 0.9 μm and 1.0 μm) across the flame boundary layer. These measurements immediately provide the integral of the soot volume fraction, $f_v\delta_s$, across the flame, $f_v\delta_s=-\lambda_o$ $ln(1-\varepsilon_o)/7$, which is replotted here in Figure 3 using coordinates similar to those in Figure 1. The factor of 7 in the above expression is recommended by Hottel and Sarofim[3] for soot. The correlation is not as good as for the soot standoff distance (Figure 2), apparently because the soot volume fraction, f_v, depends weakly on the flow time.

The faired curves in Figure 3 indicate that the fractional conversion of fuel carbon to soot, χ_s, at a fixed mass transfer rate (1) initially increases proportional to the flow time up to a height Z=0.75 m for the C_3H_6 flames, and then (2) becomes constant at greater heights.

Figure 4 shows the measured transverse temperature profiles for four C_3H_6 flames at two heights and two equivalence ratios, $\dot{m}/Z^{½}$ near 11 and 26 $g/m^{5/2}s$ respectively. Notice the dependence of profile-shape on equivalence ratio, but almost perfect similarity at fixed equivalence ratios. Theory suggests that the heat release by combustion per unit wall height increases with $Z^{1/2}$ at fixed equivalence ratio. The present data suggest that the soot and gas radiation initially increase almost linearly with height for small Z where radiation is unimportant,

but convective heat loss is important. At somewhat greater heights the radiation increases more nearly with $Z^{1/2}$ due to radiant heat loss. Ultimately the radiation will level off at very large Z after the flames become optically thick.

The similarity of combustion observed in this study greatly eases the task of analyzing experimental data and will make it much easier to tailor future detailed semi-empirical turbulent combustion models, so that their predictions exactly agree with experiment (at least for situations having $\dot{m}'' \sim Z^{1/2}$). One rarely finds such true similarity (i.e. reducible to one-dimensional behavior) in combustion, especially turbulent buoyant combustion.

We believe that these similarity relationships can be exploited to describe turbulent buoyant wall fires, with the radiative and completeness of combustion properties of the fuel characterized by the smoke point. A series of radiant and total heat feedback measurements in turbulent wall fires are planned in which the use of binary C_2H_6/C_3H_6 fuel mixtures will provide comparisons of these measurements with predictions based on the smoke point of the fuel mixture. Markstein's[2] measurements on C_3H_6 wall fires have shown that the overall heat transfer back to the surface is only about 70% of the outward heat transfer. This important effect of radiant blockage due to cold sooty gases near the wall will be studied in the planned series of C_2H_6/C_3H_6 fires.

References

1. Markstein, G.H. and de Ris, J.: Twenty-Fourth Symposium (International) on Combustion, 1747, The Combustion Institute, 1992.
2. Markstein, G.H.: Personal Communication, 1994.
3. Hottel, H.C., and Sarofim, A.F. (1962), *Radiative transfer*, McGraw-Hill, New York, p. 199.

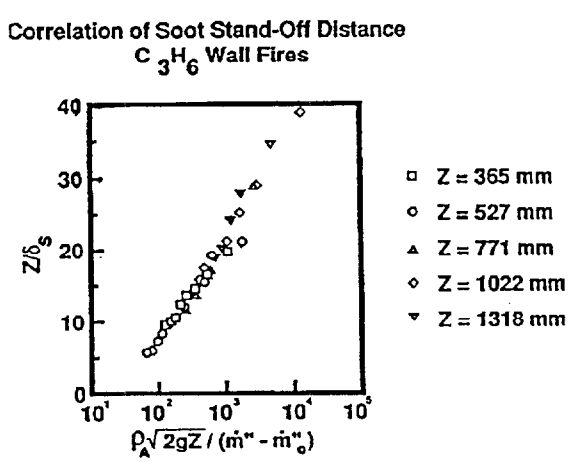

Figure 1. Height to soot layer thickness ratio correlated against inverse modified equivalence ratio.

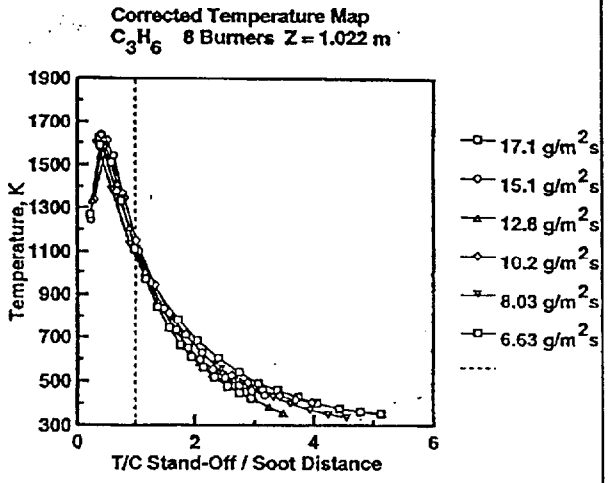

Figure. 2. Thermocouple temperatures at height Z = 1022 mm for a range of fuel mass transfer rates corrected for radiation heat loss by thermocouples inside the flames and radiative heat flux to thermocouples outside the flames. Vertical dashed line shows boundary of soot layer.

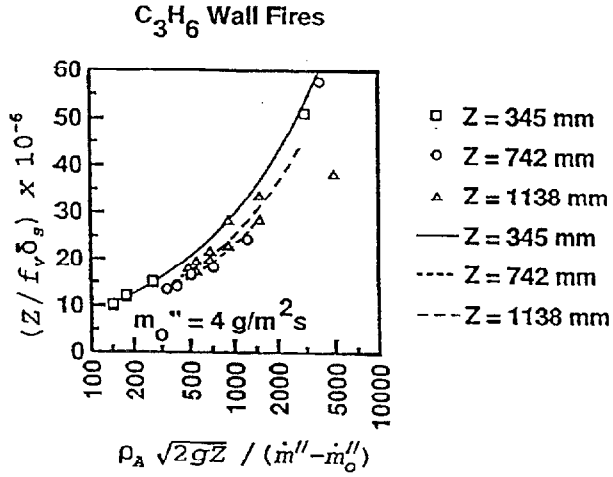

Figure 3. Ratio of height to integral of soot volume fraction across the flame correlated against inverse modified equivalence ratio.

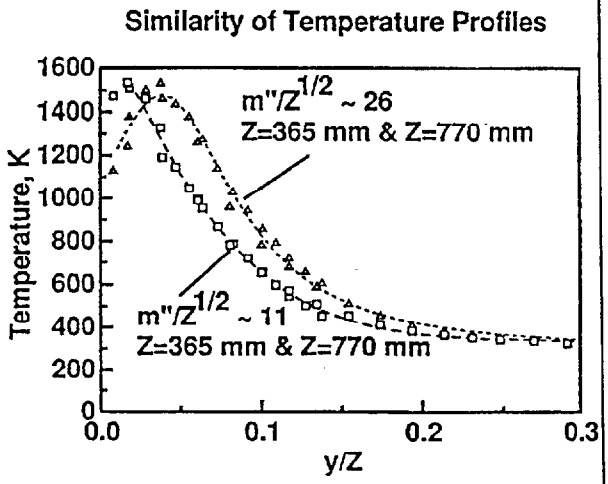

Figure 4. Temperature profile vs. normalized distance from wall.

Task 5: Methods for Developing Probability Estimates in Fire Risk Analyses (D.M. Karydas)

The Fire Risk Analysis approach establishes a performance based methodology where the performance parameter is quantified risk associated with fire hazard. The general framework of the approach includes the deterministic models of fire spread and smoke movement, the probabilistic models of the safety and control systems, and the event tree models with fire initiating event and engineered safety system functions. The associated concepts of accident prevention, consequence mitigation and hazard elimination are established. Inputs to the event tree models are provided by the deterministic models of fire spread and growth, smoke movement and deposition, and the detection/protection actuation. Additionally, the frequency of fire initiating and the success/failure probabilities of the fire safety and control systems (such as detection systems, protection systems, etc.) are provided by the probabilistic models. Adjustment to site specific fire risk assessment that deviate from the generic models are introduced at the level of accident initiation or consequence mitigation by using Bayesian inference theory. Based on this fire risk framework, a computer program is under development that can demonstrate the functional relationships of the elements of the methodology outlined and provide on-line explanation of the basic fire risk assessment terminology.

APPENDIX A

SCALING OF SOOT AND TEMPERATURES IN WALL FIRES

L. Orloff

Introduction

The present study is directed towards the measurement and analyses of optical path length, temperature profiles, and soot layer thickness in turbulent wall fires. This work parallels Markstein's[1] investigation of the radiant heat transfer blockage by cold gas and soot near the fuel surface. The results of these two studies have yielded new insights relating to the wall fire boundary layer, air/fuel mixing processes, radiative heat feedback to the fuel surface, convective heat release, and soot distribution and re-radiation in turbulent wall fires.

In earlier work, upward fire spread and steady burning along vertical PMMA slabs was investigated[2,3], and gaseous-fuel diffusion flames on flat surfaces of variable orientation, including the vertical, have been studied.[4] The role of radiative energy transfer was an essential element in understanding wall burning in these studies. Theoretical models of wall burning have also been developed at this laboratory[5,6] and elsewhere.[7-9]. However, all these models lack a predictive input for flame radiation, which controls the burning process. We believe that Markstein's and our results will provide some of the experimental data needed for the development of submodels (i.e., formulae or correlations) of wall heat transfer components for inclusion in upward spread and fire growth models.

Description of the Experiment

The pyrolysis region of a wall fire was simulated by supplying propylene to a vertical sintered porous metal surface. The burner consisted of ten 132-mm high and 380-mm wide panels topped by a 660-mm high solid metal heat transfer plate. To approach two-dimensional flow conditions as closely as possible, water cooled side walls of 150-mm depth were attached to the burner over its entire height. Further details of this apparatus are given in Markstein[1].

The fuel supply to the burner was metered by a mass flow controller and measured with an inclined manometer providing the differential pressure across the orifice of a laminar flow

element. The burner was situated in a water-cooled enclosure in a laboratory supplied with a quiescent flow of air. Product gases were vented through a passive hood directly above the burner. Fuel mass transfer rates, $\dot{m}''$, up to 60 g/m^{2}s could be obtained with three burner units operating (total height 366 mm). Activating additional burner units reduced the maximum $\dot{m}''$ due to a fixed maximum fuel supply rate.

The soot layer thickness was measured by inserting arrays of 5 mm diameter glass rods into the flame perpendicular to the wall surface and rapidly withdrawing them after a 2 second exposure to the flames. Magrides and Dobbins[10] have shown that the amount of soot deposited is proportional to the local soot volume fraction in the gas phase. Two arrays, each containing five rods were inserted for each measurement. The soot layer thickness was determined from the average length of the soot deposit on the ten rods. The 2 second exposure was chosen because shorter exposures sometimes failed to provide a well-defined soot trail, and longer exposures tended to leave thick soot deposits with poorly defined tails. The soot layer thickness is measured from the end of the rod placed against the wall to the location where the soot deposit is visually judged to have decreased to 50% of the maximum deposit on that rod. Often this position is manifested by a distinct demarcation between dark and lighter soot deposits.

The rods were laterally spaced 41 mm apart and the array was centered on the midpoint of the 381 mm wide burner surface. Typically the standard deviation of ten soot lengths was 10% of their average length. Soot layer thickness measurements were obtained for C_3H_6 supply rates, $\dot{m}''$, 4 g/m^{2}s - 60 g/m^{2}s at heights, Z, 345 mm-1138 mm above the leading edge.

Experimental Results

Fig 1 shows the variation of soot layer thickness,δ_s, with mass transfer rate at four heights.

The thickness,δ_s,approaches zero at all flame heights as the mass transfer rate approaches 4 g/m^{2}s. This critical mass transfer rate corresponds to a B-number of around 0.5, at which the flames turn blue due to a combination of wall cooling and dilution of the supplied fuel by products of combustion diffusing back to the wall. For mass transfer rates less than 4 g/m^{2}s a brown liquid rather than soot is deposited onto the glass rods.

Figure 2 shows the length ratio, Z/δ_s, correlated against the inverse modified equivalence ratio $\rho_A(2gZ)^{1/2}/(\dot{m}''-\dot{m}_o'')$. The modification of the equivalence ratio is required because the soot

vanishes and the flames become blue for mass transfer rates less than $\dot{m}_o'' = 4$ g/m^{2}s. As a result of wall cooling and dilution by the products of combustion at low mass transfer rates, the data show that the cut-off, $\dot{m}_o''$, is independent of z. The turbulent motion typically transports the luminous soot (e.g. visible flames) out into the incoming air all the way to where the mean gas temperature drops to around 1000 K. The temperature of the luminous soot at this location appears to be much hotter. The correlation says that the soot layer thickness is proportional to Z for a given ratio of entrained air, $\rho_A(2gZ^3)^{1/2}$ to supplied fuel $\dot{m}''Z$ above its blue flame value $\dot{m}_o''Z$. The correlation extends over a very wide range of flame equivalence ratios. The turbulent gas motion causes the soot to diffuse outward well into the oxygen-rich region where it encounters the entrained ambient air being drawn towards the wall.

Temperature profiles across the flame boundary layer were measured by a thermocouple rake consisting of 15 insulated Chromel-Alumel thermocouples inside 1.6 mm diameter Inconel sheaths spaced 12.6 mm on center and protruding 1 cm downward into the rising flow. The rake holder contained thermocouple connections to a fast scanning data acquisition unit. The rake was angled 56° from the normal to the burner surface for most measurements. This orientation provided 7.1 mm thermocouple spacing normal to the wall. Figures 3a and 3b show the measured thermocouple temperatures at two different heights over a wide range of mass transfer rates. Measured temperatures were averaged over 60 scans taking 95 seconds. The temperatures were not influenced by soot deposits over this measurement period.

The measured temperatures inside the flame were significantly depressed by radiation heat loss. On the other hand, the thermocouple temperatures outside the flame were significantly increased by radiant heat transfer from the flame. Using knowledge of flame radiation (reported previously) we corrected for both these effects with a simple heat transfer model to obtain the correlations shown in Figures 4a and 4b. The model is described in Appendix D.

Figures 4a and 4b show that the temperatures inside the soot zone are well correlated when the distance from the wall is normalized by the soot stand-off distance. The vertical dashed line at $y/\delta=1$ shows the boundary of the soot layer occurring at temperatures near T=1000K. Inside the soot layer, the presence of cold fuel is seen by the temperature drop near the wall. Outside the soot layer, the mixing of combustion products with the entrained air causes the corrected temperatures to asymptotically approach the ambient temperature as y/δ increases. These outer temperature profiles correlate reasonably well when plotted against $(y-\delta)/Z$.

Markstein[1] reports measurements of the extinction, ε_o,by soot of infrared radiation (at wavelengths λ_o = 0.9 μm and 1.0 μm) across the flame boundary layer. His extinction results scaled by $\dot{m}''Z^{1/2}$ are shown in Appendix E. Curve fits to these measurements immediately provide the integral of the soot volume fraction, $f_v\delta_s$, across the flame,

$$f_v\delta_s=-\lambda_o\, ln(1-\varepsilon_o)/7$$

which is replotted here in Figure 5 using coordinates similar to those in Figure 2. The factor of 7 in the above expression is recommended by Hottel and Sarofim[11] for soot. The correlation is not as good as for the soot standoff distance (Figure 2), apparently because the soot volume fraction, f_v, depends weakly on the flow time.

The faired curves in Figure 5 indicate that the fractional conversion of fuel carbon to soot, χ_s, at a fixed mass transfer rate (1) initially increases proportional to the flow time, $\sqrt{2Z/g}$, up to a height of 0.75 m for the C_3H_6 flames, and then (2) becomes constant at greater heights.

Taking the ratio of the ordinates of Figures 2 and 5 one evaluates the soot volume fraction, f_v, shown in Figure 6 for each of Markstein's C_3H_6 wall flames. These volume fractions have considerable scatter, but are reasonably independent of flow conditions. The soot volume fractions around $f_v = 10^{-6}$ provide radiant heat fluxes in general agreement with those measured in C_3H_6 flames.

Combustion Similarity for $\dot{m}''(z) \sim z^{1/2}$:

Both the equations for turbulent buoyant combustion of boundary-later diffusion flames and measured transverse profiles of velocity[7], temperature[7,8] and species concentrations[9], all show almost perfect similarity at different heights, z, in the pyrolysis zone when the supplied fuel mass transfer rate, $\dot{m}''(z)$ increases with the square root of z. For such similarity flows: (1) all macro velocities are proportional to $z^{1/2}$; (2) all transverse positions are proportional to z; while (3) all macro temperatures, densities and species concentrations are invariant at equivalent homogenous positions. It follows that the overall chemical heat release, $\dot{q}''_A$, per unit area across the flames is proportional to $z^{1/2}$ and can be expressed by

$$\dot{q}_A''(z) = z^{1/2} f(\phi) \qquad (1)$$

where $f(\phi)$ is some function of the overall fuel to entrained air equivalence ratio of the flame

$$\phi = \int_o^z \dot{m}'' \, dz / \int_o^z (-\rho v)_\infty dz \qquad (2)$$

which is determined by the value of $\dot{m}''(z)/z^{1/2}$ for a particular similarity flame. Figure 7 shows the measured transverse temperature profiles for two sets of C_3H_6 flames, at two different equivalence ratios. Notice the dependence of profile-shape on equivalence ratio, but almost perfect similarity of profiles for fixed equivalence ratio determined by $\dot{m}''(z)/z^{1/2}$. Soot and gaseous flame radiation deviate slightly from similarity, increasing at first almost linearly with height for small z, then increasing closer to $z^{1/2}$ as a result of radiant heat loss from the flames , and finally leveling off at very large z after the flames become optically thick. The convective heat loss to the wall has an opposite trend, being at first proportionately moderately large for small z, and then soon becoming negligible for large z as a result of mass transfer blowing. The combined radiative and convective flame heat transfer for the pyrolysis zone beyond z = 100 mm should be roughly similar (e.g., roughly proportional to $z^{1/2}$) for hazardous-scale fires.

This similarity of combustion greatly eases the task of analyzing experimental data and will make it much easier to tailor future detailed semi-empirical turbulent combustion models, so that their predictions exactly agree with experiment (at least for situations having $\dot{m}'' \sim (z)/z^{1/2}$). This is, so far, the only buoyant turbulent combustion situation which has been shown to be truly similar (e.g. reducible to a one-dimensional problem).

More recently we have been exploring implications of theoretical arguments which suggest that the temperature and species concentration profiles across the boundary layer should be correlated by y/Z at fixed values of the flame equivalence ratio $\dot{m}''/Z^{1/2}$.

Conclusions

1. The soot layer thickness, δ_s, is proportional to height, Z, for a given ratio of entrained air to supplied air above its blue flame value, $\dot{m}_o''Z$. The correlation extends over a very wide range of flame equivalence ratios.

2. Longitudinal flame temperature profiles inside the soot layer obtained for a range of fuel mass transfer rates are well correlated when the distance from the wall is normalized by the soot layer thickness.

3. The temperature at the boundary of the soot layer was 1000-1100 K for the C_3H_6 flames studied.

4. The fractional conversion of fuel carbon to soot, χ_s, at a fixed mass transfer rate (1) initially increases proportional to the flow time, $\sqrt{2Z/g}$, up to a height of 0.75 m for the C_3H_6 flames, and then (2) becomes constant at greater heights. We hypothesize that soot formation is proportional to available flow time for the C_3H_6 flames below 0.75 m. Above this height the available fuel carbon is increasingly oxidized.

5. Soot volume fractions, f_v, around 10^{-6} were obtained from the present δ_s measurements and Markstein's[1] extinction data. Calculated radiant heat fluxes based on this finding are in general agreement with Markstein's radiant heat transfer measurements.

6. Measured transverse temperature profiles show nearly perfect similarity of profiles for fixed equivalence ratio determined by $\dot{m}''(z)/z^{1/2}$. This discovery of a buoyant turbulent combustion similarity condition greatly simplifies the development of semi-empirical turbulent combustion models.

References

1. Markstein, G.H. and de Ris, J.:

2. Orloff, L., de Ris, J., and Markstein, G.H.: Fifteenth Symposium (International) on Combustion, 183, The Combustion Institute, 1975.

3. Orloff, L., Modak, A.T., and Alpert, R.L.: Sixteenth Symposium (International) on Combustion, 1345, The Combustion Institute, 1983.

4. de Ris, J. and Orloff, L.: Fifteenth Symposium (International) on Combustion, 175, The Combustion Institute, 1975.

5. Delichatsios, M.A.: Nineteenth Symposium (International) on Combustion, 1075, The Combustion Institute, 1983.

6. Delichatsios, M.A.: Combustion Science and Technology, 39, 195 (1984).

7. Ahmed, T. and Faeth, G.H.: Seventeenth Symposium (International) on Combustion, 1149, The Combustion Institute, 1979.

8. Mitler, H.E.: "Wall-Fire Algorithms for Mark 5.n," Appendix C, Minutes of Ad Hoc Mathematical Fire Modeling Working Group Meeting, Oct. 1984.

9. Quintiere, J., Harkleroad, M., and Hasemi, Y.: Combustion Science and Technology, 48, 191 (1986).

10. Megaridis, C.M. and Dobbins, R.A.: Twenty-Second Symposium (International) on Combustion, 353, The Combustion Institute, 1989.

11. Hottel, H.C., and Sarofim, A.F. (1962), *Radiative transfer*, McGraw-Hill, New York, p. 199,

12. Most, J.M., Sztal, B. and Delichatsios, M.A., "Turbulent Wall Fires - LDV and Temperature Measurements and Implications," 2nd International Symposium on Applications of Laser Anemometry to Fluid Mechanics, Lisbon, Portugal, July 2-4, 1984.

13. de Ris, J., Current NIST Quarterly Report.

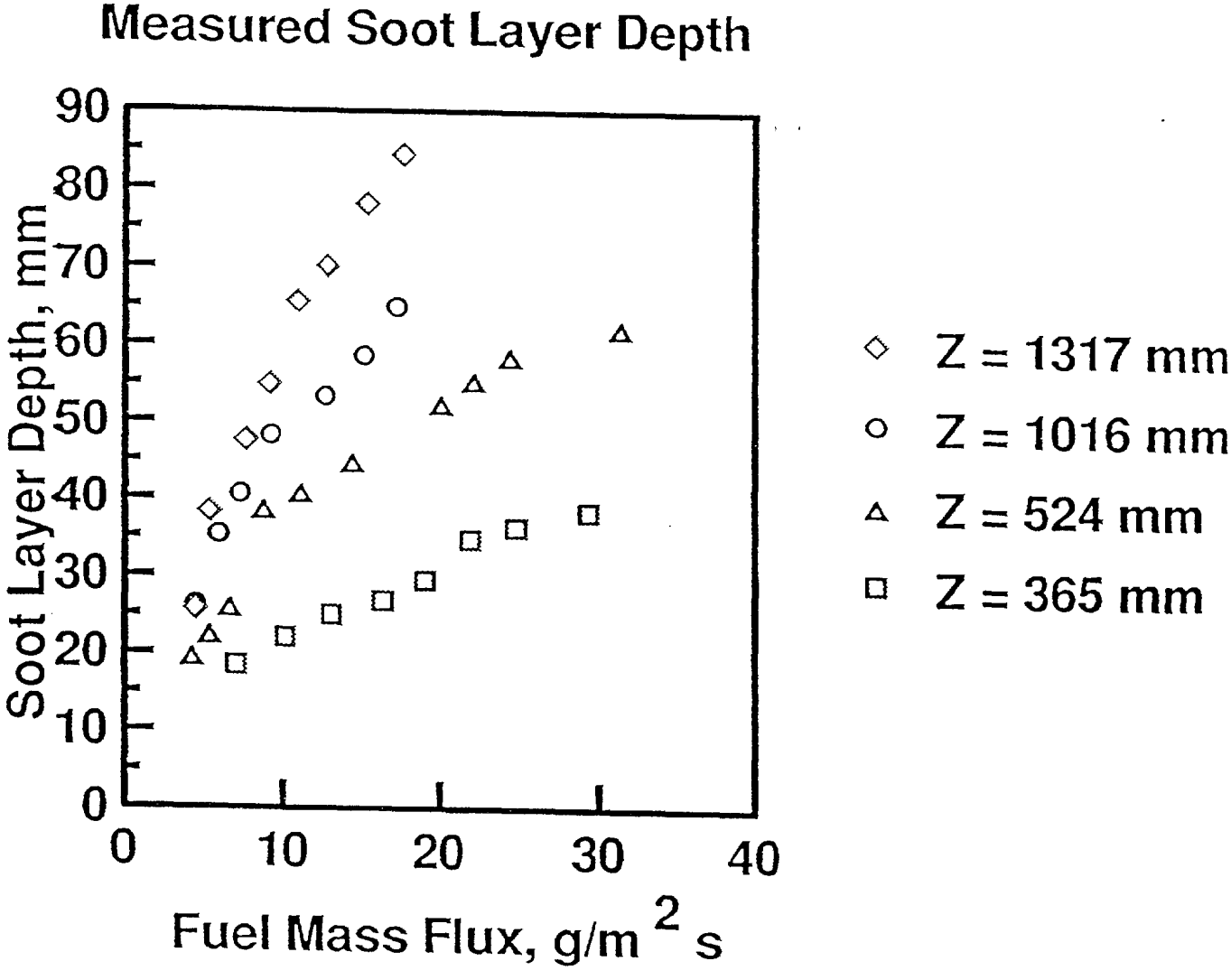

Figure 1. Variation of soot layer thickness with fuel mass flux at four heights above the leading edge.

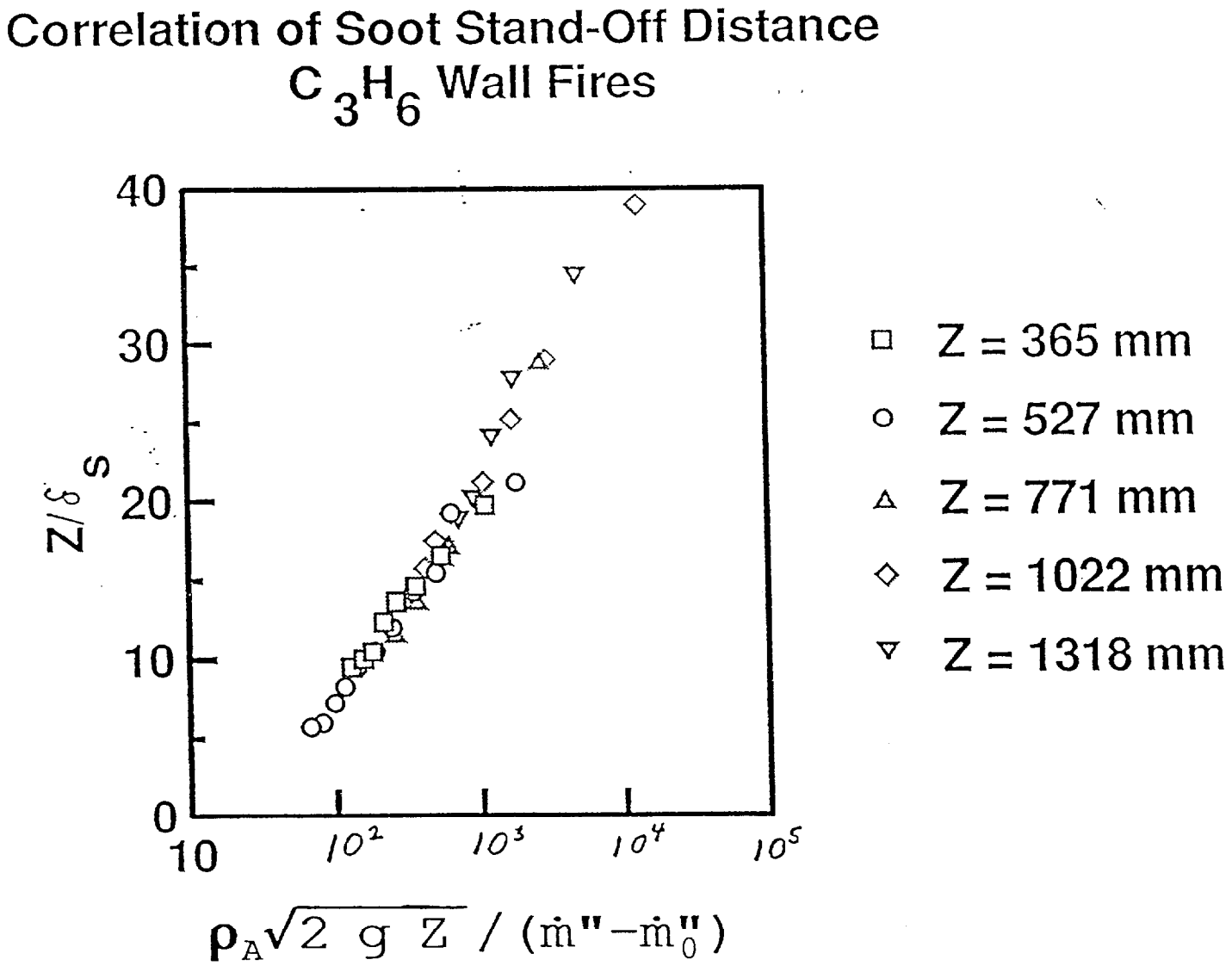

Figure 2. Height to soot layer thickness ratio correlated against inverse modified equivalence ratio.

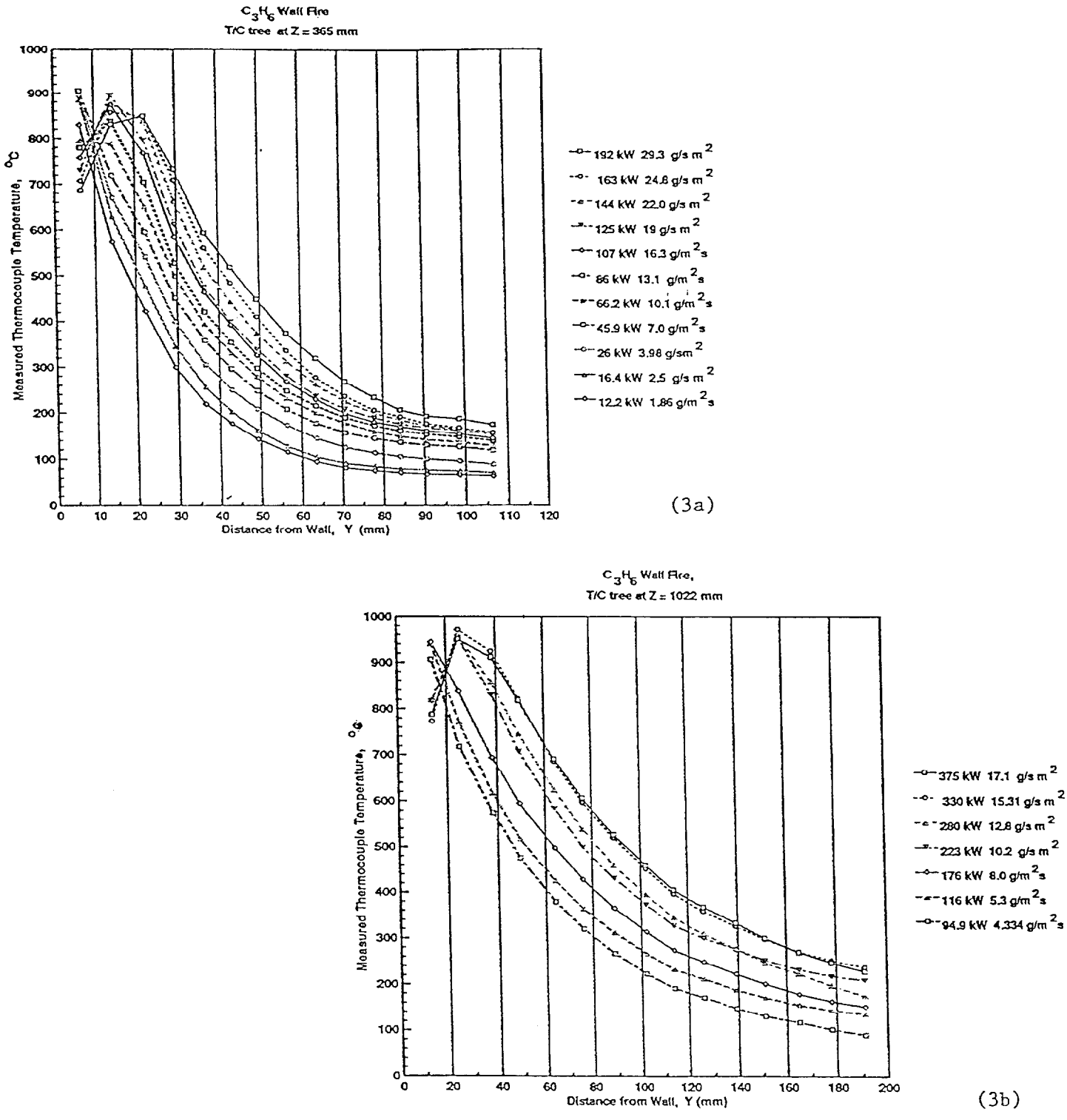

Figure 3. Measured thermocouple temperatures at heights (a) Z = 373 mm and (b) Z = 1022 mm for a range of fuel mass transfer rates.

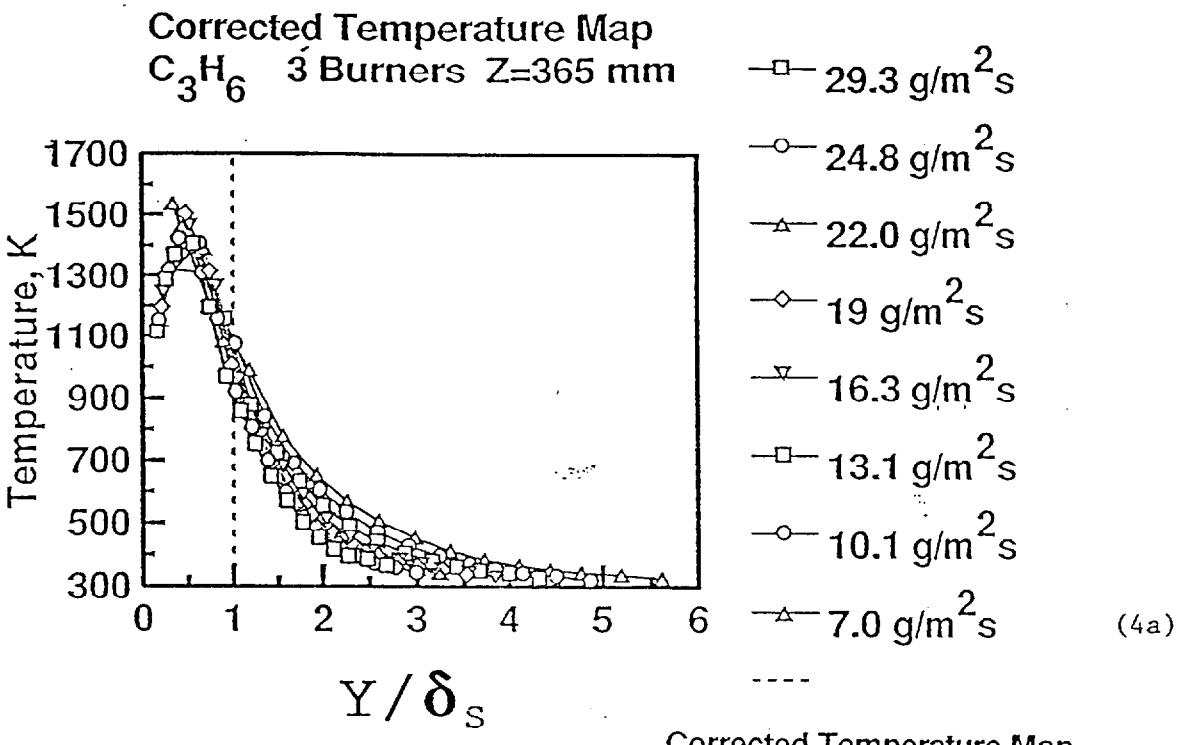

(4a)

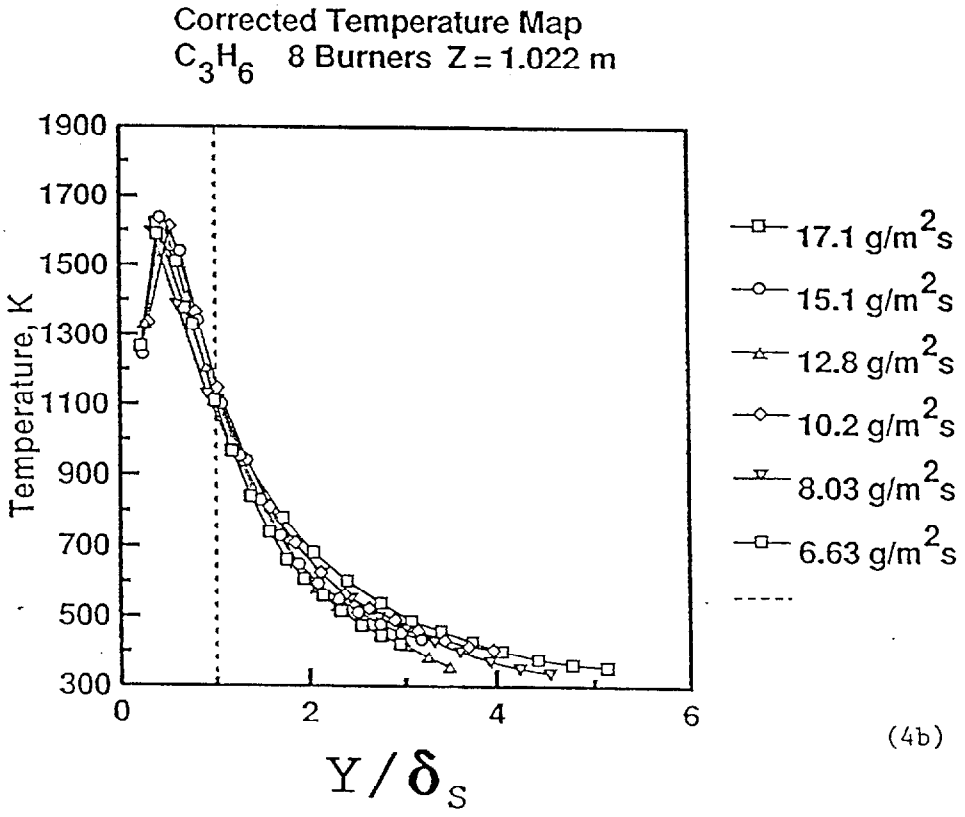

(4b)

Figure 4. Thermocouple temperatures of Figs. 3a and 3b respectively corrected for radiation heat loss by thermocouples inside the flames and radiative heat flux to thermocouples outside the flames. Vertical dashed line shows boundary of soot layer.

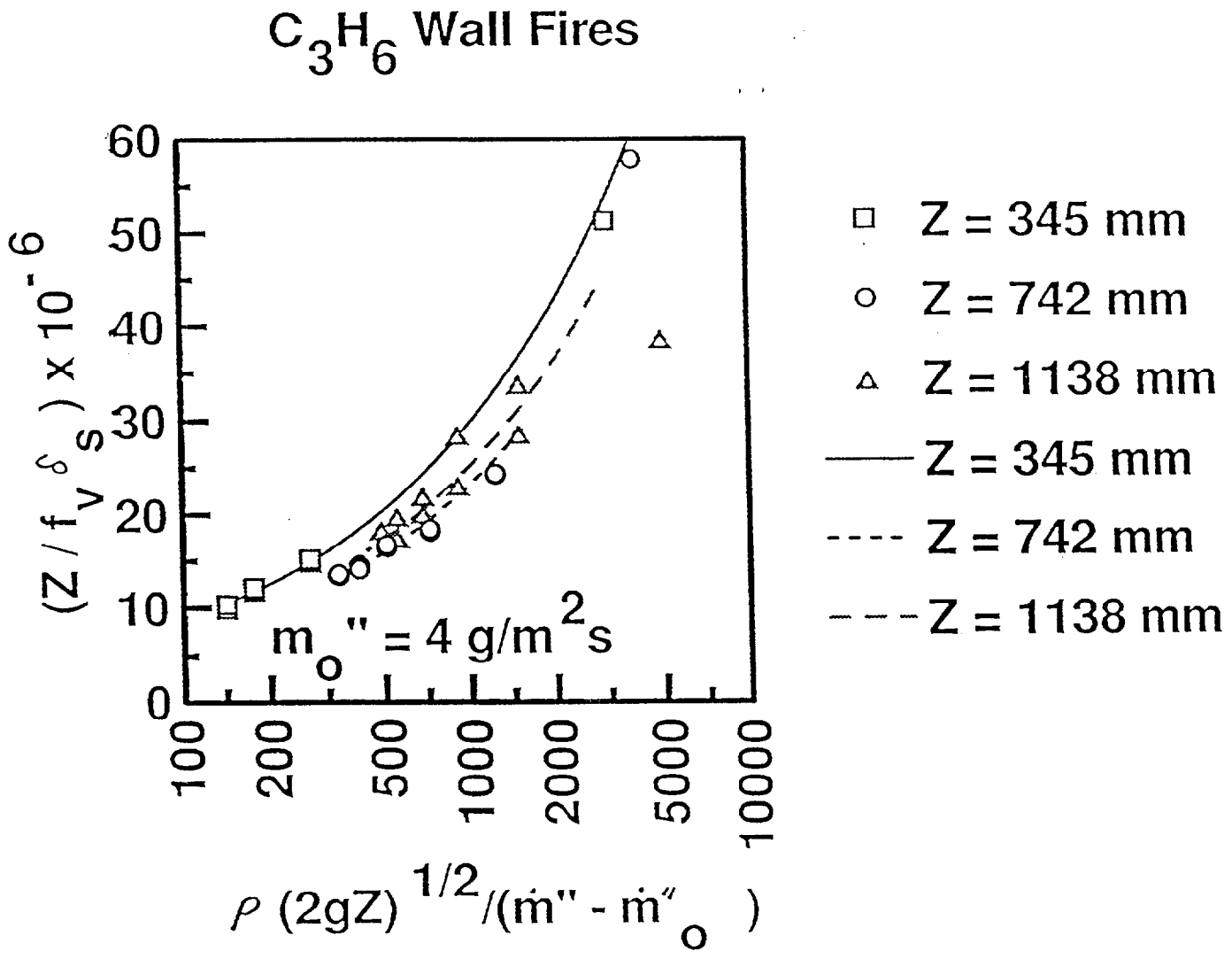

Figure 5. Ratio of height to integral of soot volume fraction across the flame correlated against inverse modified equivalence ratio.

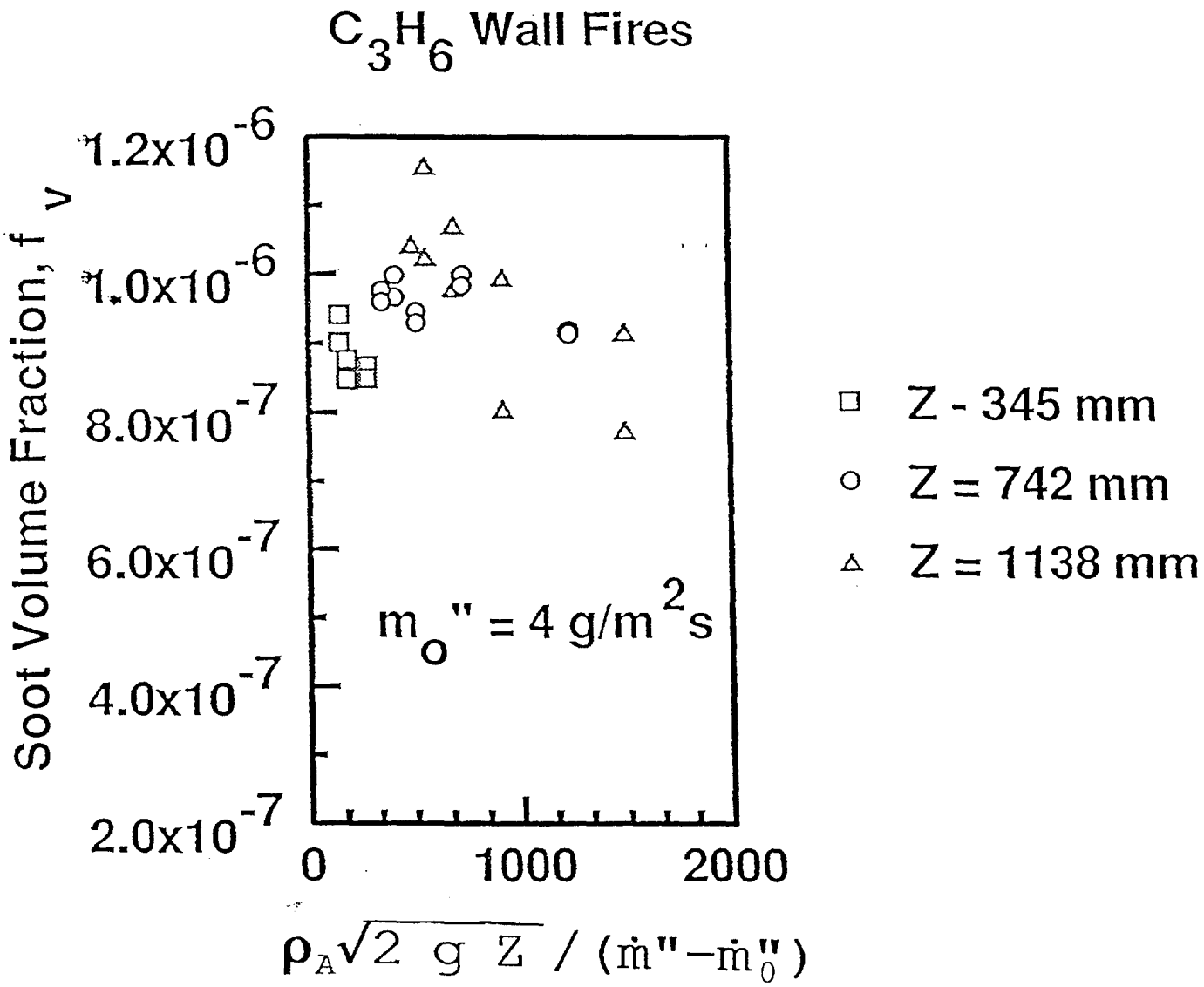

Figure 6. Soot volume fractions in C_3H_6 wall fires.

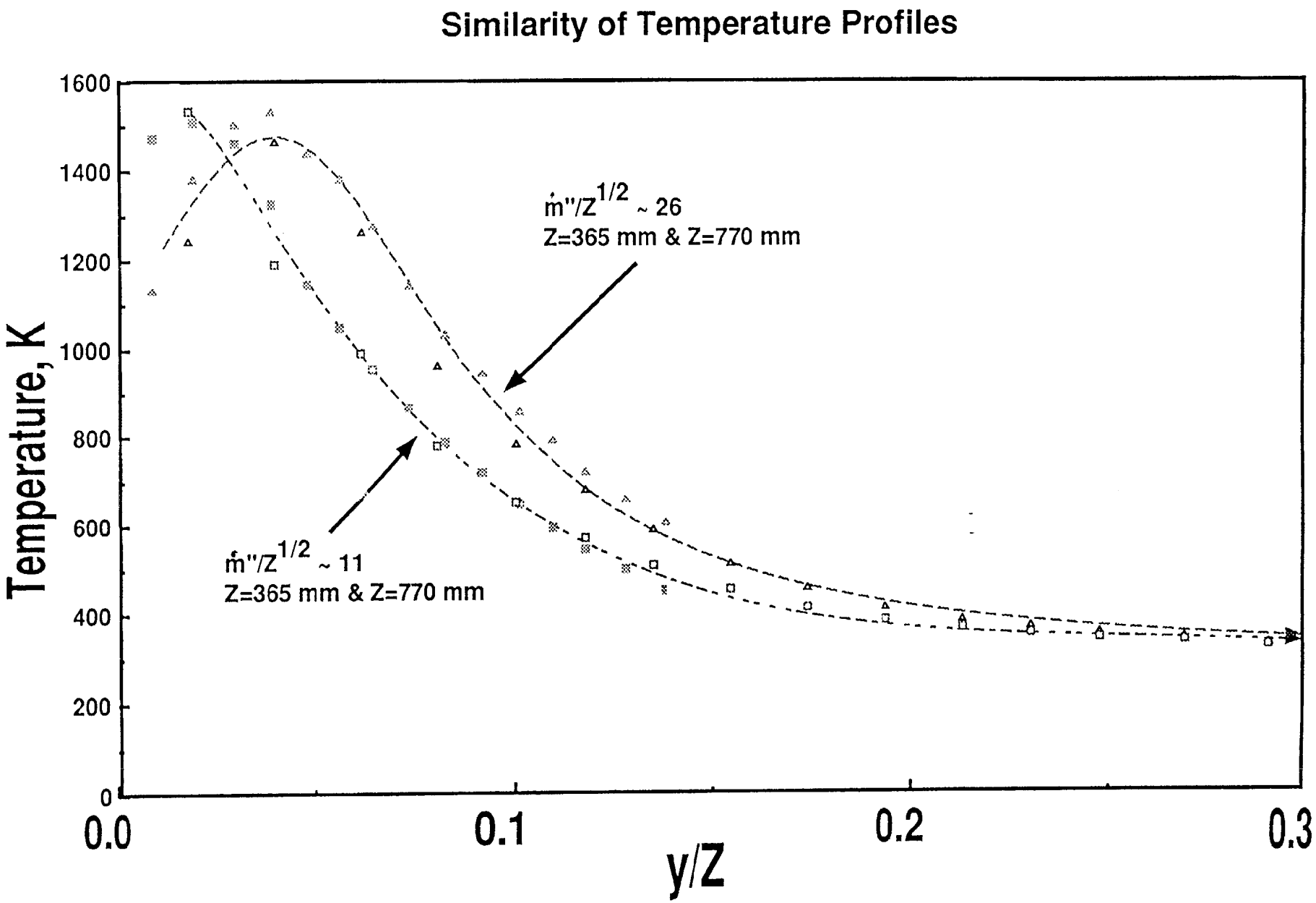

Figure 7. Measured transverse temperature profiles at different equivalence ratios

APPENDIX B

AVERAGE SOOT LAYER THICKNESS

Z = 1317.6 mm 10 burners

$\dot{Q}$ kW	$\dot{m}''$ g/m^{2}s	Soot mm
96.5	4.408	25.7
115.5	5.274	38.3
165.5	7.56	47.6
197.7	9.032	54.9
237.5	10.847	65.5
278.6	12.725	70.1
333.9	15.254	78.1
383.3	17.509	84.4

Z = 1022 mm 8 burners

$\dot{Q}$ kW	$\dot{m}''$ g/m^{2}s	Soot mm
96.5	4.407	26.2
127.7	5.832	35.3
157.8	7.21	40.6
199.5	9.115	48.2
276.6	12.635	53.3
330.3	15.09	58.6
375	17.127	64.9

Z = 527 mm 4 burners

$\dot{Q}$ kW	$\dot{m}''$ g/m^{2}s	Soot mm
54.05	6.172	24.9
89.3	10.195	27.4
104.6	11.95	34.1
133.9	15.295	37.0
173.9	19.855	43.8
216.8	24.753	50.0
275.8	31.496	55.2
330.3	37.725	63.6
382.8	43.724	72.8
458.1	52.317	88.2
544.6	62.183	92.1

Z = 365 mm 3 burners

$\dot{Q}$ kW	$\dot{m}''$ g/m^{2}s	Soot mm
191.1	29.29	38.4
158.8	24.84	36.4
143.9	21.95	34.78
125.1	19.0	29.5
105.5	16.33	26.8
84.8	13.08	25.0
65.14	10.08	22.1
45.98	6.987	18.5

Z = 771 mm 6 burners

$\dot{Q}$ kW	$\dot{m}''$ g/m^{2}s	Soot mm
293.8	22.367	66.1
224.0	17.054	56.3
166.5	12.676	46.9
155.7	11.852	44.9
75.7	5.763	26.7

APPENDIX C

CORRECTED THERMOCOUPLE MEASUREMENTS

δ_s = soot layer thickness [mm]
$\dot{m}''$ = fuel supply rate [g/m^{2}s]
Y = distance perpendicular to wall surface [mm]

C_3H_6 (3 Burners) Z = 365 mm

δ_s	39.7		35.6		32.9		30.2	
$\dot{m}''$	29.29		24.84		21.95		19.00	
Y/δ_s	T(K)	Y/δ_s	T(K)	Y/δ_s	T(K)	Y/δ_s	T(K)
0.160	1113.9	0.178	1153.1	0.193	1151.9	0.211	1196.7
0.360	1370.9	0.401	1423.4	0.434	1463.0	0.474	1502.6
0.559	1405.9	0.624	1407.6	0.676	1389.2	0.737	1315.2
0.739	1196.6	0.825	1158.6	0.893	1083.3	0.974	1006.3
0.919	971.4	1.026	922.9	1.110	861.1	1.211	800.6
1.079	858.1	1.204	807.9	1.303	749.4	1.422	691.8
1.239	755.1	1.383	701.9	1.496	652.6	1.632	607.0
1.418	649.4	1.584	598.4	1.713	567.8	1.869	527.7
1.598	572.7	1.784	517.7	1.930	498.2	2.106	466.8
1.778	503.0	1.985	461.8	2.147	446.0	2.343	426.0
1.958	455.1	2.186	418.2	2.365	409.2	2.580	396.7
2.118	417.0	2.364	397.1	2.558	387.5	2.791	376.9
2.277	396.7	2.543	374.4	2.751	367.8	3.001	362.6
2.477	387.2	2.766	360.6	2.992	356.3	3.264	352.7
2.677	368.2	2.989	344.8	3.233	342.5	3.528	338.6

δ_s	27.7		24.6		21.8		19.0	
$\dot{m}''$	16.33		13.08		10.08		7.0	
Y/δ_s	T(K)	Y/δ_s	T(K)	Y/δ_s	T(K)	Y/δ_s	T(K)
0.230	1245.3	0.258	1287.5	0.291	1320.4	0.335	1534.5
0.516	1465.3	0.580	1394.6	0.654	1308.8	0.753	1191.4
0.803	1265.1	0.902	1159.2	1.017	1075.3	1.172	992.0
1.062	964.1	1.192	880.3	1.345	841.9	1.549	780
1.320	784.1	1.482	726.1	1.672	692.8	1.925	652.9
1.549	682.0	1.740	633.6	1.962	607.1	2.260	570.4
1.779	590.8	1.997	556.5	2.253	536.6	2.595	508.0
2.037	512.8	2.287	488.9	2.580	472.6	2.972	454.1
2.295	457.7	2.577	442.6	2.907	428.8	3.349	412.8
2.554	413.9	2.867	405.9	3.234	396.2	3.725	384.3
2.812	386.4	3.157	379.8	3.561	370.1	4.102	366.4
3.041	370.8	3.415	362.9	3.852	354.3	4.437	353.3
3.271	356.2	3.673	350.3	4.143	342.1	4.772	343.4
3.558	345.1	3.995	341.2	4.506	333.9	5.190	336.6
3.845	330.6	4.317	327.1	4.869	320.4	5.609	324.8

C_3H_6 (6 Burners) Z = 771 mm

δ_s	66.2		66.0		65.1		56.7	
$\dot{m}''$	22.49		22.37		21.80		17.05	
Y/δ_s	T(K)		Y/δ_s	T(K)	Y/δ_s	T(K)	Y/δ_s	T(K)
0.096	1133.8		0.096	1233.8	0.097	1357.9	0.112	1342.7
0.216	1382.4		0.217	1423.4	0.219	1455.3	0.252	1482.6
0.336	1504.4		0.337	1499.4	0.341	1486.4	0.392	1517.0
0.444	1533.3		0.445	1491.8	0.451	1456.1	0.518	1454.9
0.552	1439.3		0.553	1357.6	0.560	1337.4	0.644	1296.6
0.648	1382.2		0.650	1285.9	0.658	1269.7	0.756	1212.1
0.744	1278.6		0.746	1180.4	0.755	1172.4	0.868	1093.5
0.852	1143.9		0.854	1059.7	0.865	1063.9	0.994	1001.4
0.960	1034.6		0.962	986.3	0.975	980.8	1.120	918.0
1.068	947.2		1.071	902.9	1.084	897.8	1.246	834.6
1.176	858.4		1.179	818.7	1.194	816.2	1.372	761.9
1.272	793.3		1.275	762.7	1.291	753.4	1.484	703.9
1.368	722.1		1.371	701.3	1.389	694.4	1.596	650.2
1.488	660.4		1.492	637.4	1.511	634.6	1.736	595.0
1.608	606.7		1.612	577.2	1.633	576.5	1.876	541.9

δ_s	46.8		44.7		36.1	
$\dot{m}''$	12.68		11.85		8.75	
Y/δ_s	T(K)		Y/δ_s	T(K)	Y/δ_s	T(K)
0.136	1435.7		0.142	1473.2	0.176	1520.3
0.306	1517.6		0.320	1509.9	0.396	1436.3
0.475	1488.9		0.498	1461.2	0.616	1338.1
0.628	1350.7		0.658	1327.1	0.814	1177.0
0.781	1160.0		0.818	1145.8	1.012	1018.6
0.917	1053.1		0.960	1049.2	1.188	932.8
1.052	958.0		1.102	955.8	1.364	853.0
1.205	874.3		1.262	867.7	1.563	773.8
1.358	808.7		1.422	787.6	1.761	704.7
1.511	741.1		1.582	719.6	1.959	641.2
1.664	671.4		1.742	649.5	2.157	579.2
1.799	619.6		1.884	595.5	2.333	534.8
1.935	570.6		2.026	545.2	2.509	492.6
2.105	522.1		2.204	500.0	2.729	450.8
2.275	471.0		2.382	452.5	2.949	407.3

C_3H_6 9 Burners Z = 1.022 m

δ_s	64.9	60.3	54.9	48.2
$\dot{m}''$	17.13	15.10	12.80	10.18

Y/δ_s	T(K)	Y/δ_s	T(K)	Y/δ_s	T(K)		
0.216	1266.3	0.232	1244.0	0.255	1334.2	0.291	1335.9
0.385	1589.3	0.414	1635.9	0.455	1616.5	0.519	1611.8
0.586	1509.6	0.630	1541.3	0.692	1410.5	0.789	1366.7
0.755	1331.0	0.812	1343.0	0.893	1206.5	1.017	1148.6
0.986	1109.7	1.061	1101.5	1.166	1002.2	1.328	942.5
1.171	968.3	1.260	953.8	1.385	865.2	1.577	812.0
1.371	841.1	1.475	831.6	1.621	747.7	1.847	710.1
1.572	741.6	1.691	731.0	1.858	653.4	2.117	627.2
1.757	662.7	1.890	651.3	2.077	582.3	2.366	562.9
1.942	608.8	2.089	596.4	2.295	532.3	2.615	524.5
2.142	560.8	2.304	551.8	2.532	489.6	2.884	492.2
2.327	516.6	2.503	513.5	2.751	447.6	3.133	460.7
2.543	475.3	2.735	479.2	3.006	417.6	3.424	433.9
2.743	446.7	2.951	454.6	3.243	383.9	3.694	415.7
2.943	422.7	3.166	436.1	3.480	355.5	3.963	405.4

δ_s	42.0	37.2
$\dot{m}''$	8.03	6.63

Y/δ_s	T(K)	Y/δ_s	T(K)
0.334	1595.2	0.376	1620.7
0.596	1385.0	0.671	1377.3
0.905	1129.8	1.021	1111.0
1.168	968.6	1.316	939.5
1.525	817.3	1.719	781.6
1.811	714.7	2.041	684.0
2.121	623.8	2.390	603.8
2.430	552.6	2.740	539.1
2.716	497.9	3.062	489.0
3.002	463.3	3.384	460.2
3.312	428.4	3.733	428.3
3.598	399.4	4.056	401.1
3.931	370.7	4.432	377.0
4.241	350.5	4.781	361.9
4.551	336.5	5.130	354.6

APPENDIX D

EFFECTS OF FLAME RADIATION AND SURFACE RERADIATION ON THERMOCOUPLE GAS TEMPERATURE MEASUREMENTS IN AND NEAR FLAMES

Thermocouples are often used to measure local gas temperatures both inside and near to flames. However, the radiative heat transfer from the flames increases the thermocouple temperature, while the radiative heat loss from the hot thermocouple surface decreases its temperature. In steady state, the convective heat transfer to the thermocouple from the gas flowing over the thermocouple must equal the radiative heat loss from its surface minus the rate of heat gain from nearby flames, or

$$h(T_g - T) = \sigma\ (T^4 - T_\infty^4)\ - \epsilon_f\ \sigma\ (T_f^4 - T_\infty^4)$$

per unit thermocouple surface area. Here, T, T_g, and T_f, respectively, are the thermocouple, gas, and effective flame radiation temperatures; h is the convective heat transfer coefficient; σ is the Stefan-Boltzmann constant 5.7 W/cm^2 (1000K)^4; and ϵ_f is the average flame emissivity, as viewed by the thermocouple. We implicitly assume that the thermocouple is coated by a thin layer of black soot, causing it to have unit surface absorptivity and emissivity. Solving for T_g, one has

$$T_g = T + \sigma/h\ (T^4 - T_\infty^4)\ - \epsilon_f/h\ \sigma\ (T_f^4 - T_\infty^4)\ .$$

Convective Heat Transfer

Our thermocouples point downward into the rising hot flow. Eckert and Drake (1972) provides the convective heat transfer formulas:

$$Nu = hd/k = [0.43 + 0.50\ Re^{0.5}]Pr^{0.38}\ \text{(cylinders in cross flow)}$$

$$Nu = hd/k = 2.00 + 0.236\ Re^{0.606}Pr^{0.5}\ \text{(spheres)}$$

Both these formulas yield a Nusselt number around 4 for a Reynolds number

$$R_e = ud/\nu \cong \sqrt{2gZ}\ d/\nu \cong 45$$

Evaluated for a d = 0.15 cm diameter thermocouple in a one meter high (Z = 1m) flame at 1300 K. The Reynolds number is quite uniform across the flame because the temperature dependence of the kinematic viscosity, ν, causes it to decrease almost proportionally to the velocity μ, as the velocity decreases from its maximum value in the flame to its inward directed entrainment value in the cold gas surrounding the flame. Thus, modeling the thermocouple by either a cylinder or sphere, one has

$$h = N\mu\ k/d \cong 4\ k_\infty (T/T_\infty)^{0.75}/d = 0.01 (T/T_\infty)^{0.8}\ W/cm^2\ K$$

which takes into account the temperature dependence of the gas thermal conductivity, k.

Flame Radiances

Consider a planar flame of uniform thickness, δ, adjacent to a vertical wall. It is assumed that the effective flame radiation temperature, T_f, is independent of the distance, y, from the wall, while the probability of finding a flame at position y decreases with y, so that the time-averaged flame absorption-emission coefficient α (y) decreases with y and becomes zero for $y > \delta$. Defining the local optical depth normal to the wall

$$\eta = \int_o^y \alpha\ dy$$

The flame radiances along rays at an angle ϕ w.r.t. the normal become

$$N_+ (\eta, \phi) = \frac{\sigma}{\pi} (T_f^4 - T_\infty^4) (1 - e^{-\eta \sec\phi}) \qquad outward$$

$$N_- (\eta, \phi) = \frac{\sigma}{\pi} (T_f^4 - T_\infty^4) (1 - e^{-(\eta_m - \eta)\sec\phi}) \qquad inward$$

where η_m is the maximum value of η corresponding to $y = \delta$. The outward flame radiance, N_+ continues constant along a ray extending beyond the flame thickness $y > \delta$. It only depends on the angle ϕ. The inward flame radiance occurs only inside the flame, $y < \delta$.

Radiation to a Thermocouple Inside the Flame

In general, the radiant heat transfer, $\dot{q}$", impinging on a surface, is

$$\dot{q}'' = \int N(\phi) \cos\phi \, d\Omega$$

where Ω is the solid angle and ϕ is the angle of a ray to the outward normal. In the case of a planar flame between two parallel surfaces, the integral over ϕ can be approximated by evaluating $N(\phi \cos\phi$ at its "mean beam" value ($\phi = \pi/3$) and multiplying it by the solid angle $\Omega = 2\pi$ facing the flame, to obtain

$$\dot{q}'' = \overline{N(\phi)\cos\phi} \cdot \Omega = \frac{\sigma}{\pi} (T_f^4 - T_\infty^4) \frac{(1-e^{1.8\eta})}{2} 2\pi = \sigma (T_f^4 - T_\infty^4) (1-e^{-1.8\eta})$$

where η is the flame optical depth normal to the surface. The approximation is slightly improved by setting $\sec\phi = 1.8$ instead of 2 in the exponent.

To evaluate the heat transfer to a spherical thermocouple of diameter d located inside the flame, we calculate the total inward and outward radiation impinging on a thin circular disk of area $\pi d^2/4$, parallel to the wall, to obtain the average heat transfer, $\dot{q}$", per unit thermocouple area

$$\dot{q}'' = \frac{\dot{q}_+ + \dot{q}_-}{\pi d^2} = \frac{\pi d^2/4}{\pi d^2} \sigma \left(T_f^4 - T_\infty^4\right) \left[(1-e^{-1.8\eta}) + (1-e^{-1.8(y_m-y)})\right]$$

This radiation is maximum at the center of the flame $y = \eta_m/2$ and is minimum at both the inner edges $y = 0, \eta_m$:

$$\dot{q}''_{max} = \frac{\sigma}{2} \left(T_f^4 - T_\infty^4\right) \left(1-e^{-0.9\eta_m}\right)$$

$$\dot{q}''_{min} = \frac{\sigma}{4} \left(T_f^4 - T_\infty^4\right) \left(1-e^{-1.8\eta_m}\right)$$

which become equal for optically thin flames $\eta_m \rightarrow 0$.

Radiation to a Thermocouple Outside the Flame

For $y > \delta$ the radiances emitted by the flame remain constant along each ray. However, the lateral side walls limit the extent of the flame and reduce the total solid angle of the flame as viewed by the thermocouple. Consider a uniform flame of thickness δ in the form of a circular slab of radius R viewed by a thermocouple disk of area $\pi d^2/4$ located a distance y along the axis from the flame. Assume δ/y and d/y are very small.

The total solid angle of the flame, Ω, as viewed from y is

$$\Omega_1 = 2\pi \int_o^{\theta_1} \sin\theta d\theta = 2\pi\ (1-COS\theta_1)\ .$$

The angle of the "mean beam" θ_2 subtends half this solid angle,

$$\Omega_2 = \Omega_1/2 = \pi\ (1-COS\theta_1) = 2\pi\ (1-\cos\theta_2)$$

so that

$$\cos\theta_2 = (1 + \cos\theta_1)/2 = (1 + y/\sqrt{y^2+\pi^2}\ )/2$$

Evaluating $N(\phi)\cos\phi$ along the "mean beam" the heat transfer to the thermocouple (i.e., disk) per unit thermocouple area becomes

$$\dot{q}'' = \frac{\pi d^2/4}{\pi d^2} N(\theta_2)\ \cos\theta_2\ \Omega_1$$

$$= \frac{\sigma}{4\pi} \left(T_f^4 - T_\infty^4\right) \left(1-e^{0.9\eta_m \sec\theta_2}\right) \cos\theta_2 \cdot 2\pi\ (1-\cos\theta_1)$$

$$= \frac{\sigma}{4} \left(T_f^4 - T_\infty^4\right) \left(1-e^{0.9\eta_m \sec\theta_2}\right) \frac{R^2}{(y^2 + R^2)}$$

where

$$\sec\theta_2 = 2\sqrt{y^2 + R^2}\ /\ (y + \sqrt{y^2 + R^2})$$

After letting R go to infinity, this heat transfer smoothly matches the inside flame value at the flame edge y = δ.

Flame Radiation Inside and Outside the Flame

The above results can be combined into a single expression

$$\dot{q}'' = \frac{\sigma}{4}\left(T_f^4 - T_\infty^4\right)\left(\frac{R^2}{y^2 + R^2}\right) f(y)$$

$$f(y) = \left(1 - e^{0.9\bar{\alpha}\, y \sec\theta_2}\right) + h(\delta - y)\left(1 - e^{0.9\bar{\alpha}\,(\delta - y)\sec\theta_2}\right)$$

APPENDIX E

MARKSTEIN'S SOOT EXTINCTION MEASUREMENTS

Markstein's[1] measurements of the extinction, ε_o by soot of infrared radiation (at wavelengths λ_o = 0.9 μm and 1.0 μm) across the flame boundary layer shows that soot optical depth scaled by $\dot{m}''Z^{1/2}$ is curve-fitted by $[A/(50 + \dot{m}'')]\ \{(\dot{m}''+\dot{m}_o'')^2 - (\dot{m}_o'' + 4)^2]^{1/2}$, where $\dot{m}_o'' = 4$ g/m^{2}s, and A = 0.6, 1.35 and 1.7 at Z = .345 m, ;742, and 1.7 at Z = 0.345 m, 0.742 m, and 1.138 m, respectively.

NIST-114
(REV. 11-94)
ADMAN 4.09

U.S. DEPARTMENT OF COMMERCE
NATIONAL INSTITUTE OF STANDARDS AND TECHNOLOGY

(ERB USE ONLY)
ERB CONTROL NUMBER | DIVISION
PUBLICATION REPORT NUMBER | CATEGORY CODE

MANUSCRIPT REVIEW AND APPROVAL

INSTRUCTIONS: ATTACH ORIGINAL OF THIS FORM TO ONE (1) COPY OF MANUSCRIPT AND SEND TO THE SECRETARY, APPROPRIATE EDITORIAL REVIEW BOARD.

PUBLICATION DATE: October 1997
NUMBER PRINTED PAGES:

TITLE AND SUBTITLE (CITE IN FULL)

Prediction of Fire Dynamics

CONTRACT OR GRANT NUMBER
60NANB1D1177

TYPE OF REPORT AND/OR PERIOD COVERED
Final Report and Quarterly Report
July 1, 1994 - August 28, 1994

AUTHOR(S) (LAST NAME, FIRST INITIAL, SECOND INITIAL)
John de Ris
Factory Mutual Research Corporation
Norwood, MA 02062

PERFORMING ORGANIZATION (CHECK (X) ONE BLOCK)
- [ ] NIST/GAITHERSBURG
- [ ] NIST/BOULDER
- [ ] JILA/BOULDER

LABORATORY AND DIVISION NAMES (FIRST NIST AUTHOR ONLY)

SPONSORING ORGANIZATION NAME AND COMPLETE ADDRESS (STREET, CITY, STATE, ZIP)
U.S. Department of Commerce
National Institute of Standards and Technology
Gaithersburg, MD 20899

PROPOSED FOR NIST PUBLICATION
- [ ] JOURNAL OF RESEARCH (NIST JRES)
- [ ] J. PHYS. & CHEM. REF. DATA (JPCRD)
- [ ] HANDBOOK (NIST HB)
- [ ] SPECIAL PUBLICATION (NIST SP)
- [ ] TECHNICAL NOTE (NIST TN)
- [ ] MONOGRAPH (NIST MN)
- [ ] NATL. STD. REF. DATA SERIES (NIST NSRDS)
- [ ] FEDERAL INF. PROCESS. STDS. (NIST FIPS)
- [ ] LIST OF PUBLICATIONS (NIST LP)
- [ ] NIST INTERAGENCY/INTERNAL REPORT (NISTIR)
- [ ] LETTER CIRCULAR
- [ ] BUILDING SCIENCE SERIES
- [ ] PRODUCT STANDARDS
- [ ] OTHER

PROPOSED FOR NON-NIST PUBLICATION (CITE FULLY) [ ] U.S. [ ] FOREIGN

PUBLISHING MEDIUM
- [ ] PAPER
- [ ] CD-ROM
- [ ] DISKETTE (SPECIFY)
- [ ] OTHER (SPECIFY)

SUPPLEMENTARY NOTES

ABSTRACT (A 2000-CHARACTER OR LESS FACTUAL SUMMARY OF MOST SIGNIFICANT INFORMATION. IF DOCUMENT INCLUDES A SIGNIFICANT BIBLIOGRAPHY OR LITERATURE SURVEY, CITE IT HERE. SPELL OUT ACRONYMS ON FIRST REFERENCE.) (CONTINUE ON SEPARATE PAGE, IF NECESSARY.)

This report describes a transient ceiling jet heat transfer model and correlations of the temperature and soot distributions across vertical buoyant turbulent boundary layers generated by propylene-air diffusion flames set up to simulate wall-fires.

The ceiling jet heat transfer model describes the transient heat-up of the ceiling and cool-down of gases as they flow downstream beneath a ceiling. An analytic (Laplace transform) solution describes how the ceiling and gas temperatures change with distance and time for a given ceiling flow velocity, layer depth, and mass flow per unit width. In certain cases the results can be approximated by simple algebraic formulas employing log-mean temperatures. With those results we are now in a position to formulate general models as well as for turbulent wall-fire combustion providing expressions for the flame heat transfer rates, needed for predicting wall-fire burning-and upward spread rates

KEY WORDS (MAXIMUM OF 9; 28 CHARACTERS AND SPACES EACH; SEPARATE WITH SEMICOLONS; ALPHABETIC ORDER; CAPITALIZE ONLY PROPER NAMES)
ceiling jets; diffusion flames; heat transfer; fire models; flame spread; soot; temperature; turbulent flames; walls

AVAILABILITY
- [x] UNLIMITED
- [ ] FOR OFFICIAL DISTRIBUTION - DO NOT RELEASE TO NTIS
- [ ] ORDER FROM SUPERINTENDENT OF DOCUMENTS, U.S. GPO, WASHINGTON, DC 20402
- [x] ORDER FROM NTIS, SPRINGFIELD, VA 22161

NOTE TO AUTHOR(S): IF YOU DO NOT WISH THIS MANUSCRIPT ANNOUNCED BEFORE PUBLICATION, PLEASE CHECK HERE. [ ]

ELECTRONIC INFORMS